Cooperation of two opposite flagella allows high-speed swimming and active turning in zoospores

Quang D. Tran,[1,*] Eric Galiana,[2] Philippe Thomen,[1] Céline Cohen,[1]
François Orange,[3] Fernando Peruani,[4,5] and Xavier Noblin[1,†]

[1] *Université Côte d'Azur, CNRS UMR 7010, Institut de Physique de Nice (INPHYNI), 06108 Nice, France*
[2] *Université Côte d'Azur, INRAE UMR 1355, CNRS UMR 7254, Institut Sophia Agrobiotech (ISA), 06903 Sophia Antipolis, France*
[3] *Université Côte d'Azur, Centre Commun de Microscopie Appliquée (CCMA), 06108 Nice, France*
[4] *Université Côte d'Azur, CNRS UMR 7351, Laboratoire J.A. Dieudonné (LJAD), 06108 Nice, France*
[5] *CY Cergy Paris Université, CNRS UMR 8089, Laboratoire de Physique Théorique et Modélisation, 95302 Cergy-Pontoise, France*

(Dated: May 20, 2021)

Phytophthora species cause diseases in a large variety of plants and represent a serious agricultural threat, leading, every year, to multibillion dollar losses. Infection occurs when these biflagellated zoospores move across the soil at their characteristic high speed and reach the roots of a host plant. Despite the relevance of zoospore spreading in the epidemics of plant diseases, it is not known how these zoospores swim and steer with two opposite beating flagella. Here, combining experiments and modeling, we show how these two flagella contribute to generate thrust when beating together, and identify the mastigonemes-attached anterior flagellum as the main source of thrust. Furthermore, we find that steering involves a complex active process, in which the posterior flagellum is stopped, while the anterior flagellum keeps on beating, as the zoospore reorients its body. Our study is a fundamental step towards a better understanding of the spreading of plant pathogens' motile forms, and shows that the motility pattern of these biflagellated zoospores represents a distinct eukaryotic version of the celebrated "run-and-tumble" motility class exhibited by peritrichous bacteria.

Life of swimming microorganisms in viscosity-dominant world has been of great interest in biophysics research. The problems on microbial locomotion of those tiny individual flagellated swimmers are still far to be fully understood. There have been a multitude of theoretical and experimental models of microswimmers that study the hydrodynamics of the individual and collective motions of those cells [1, 2]. These swimming cells can be categorized into two groups: eukaryotes (having nuclei) and prokaryotes (no nuclei). *Escherichia coli* is one of the most studied prokaryotic swimmers, which possesses a passive helical flagellum controlled by a rotary motor attached to the cell body [3]. Eukaryotic microswimmers, such as green algae *Chlamydomonas* [4, 5] and spermatozoa [6, 7], have active and flexible flagella along which molecular motors are distributed. Here, we introduce a new type of microswimmer, named *Phytophthora* zoospores, which has two different flagella collaborating for unique swimming and turning mechanisms (**Figure 1**(a)).

Phytophthora is a genus of eukaryotic and filamentous microorganisms. They are classified as oomycetes and grouped in the kingdom of the Stramenopiles with the heterokont algae (such as diatoms and brown algae) [8, 9]. A number of *Phytophthora* species are plant pathogens and cause tremendous damages to agro- and eco-systems [10, 11]. Nowadays, *Phytophthora* diseases are responsible for a big impact on economies with billions of dollars of damages each year and remain a threat to the food security worldwide [12–14]. The diseases are pervasive as they release swimming biflagellated spores called "zoospores" which initiates the spreading through water. These zoospores are able to accumulate speed up to $250\,\mu\mathrm{m\,s^{-1}}$ through thin water films, water droplets on leaves, or through pores within moist soils. To facilitate the spreading, their cell bodies store an amount of energy (mycolaminarin, lipid) allowing them to swim continuously for several hours [14]. When the zoospores reach plant roots, they stop swimming and loose their flagella to produce a primary cell wall and become germinative cysts which are able to penetrate into the host tissue. Then, they start a hyphal growth inside the infected plant. In this study, we investigate the telluric species *P. parasitica*, a polyphagous pathogen attacking a wide range of hosts such as tobacco, onion, tomato, ornamentals, cotton, pepper, citrus plants and forest ecosystems [15].

Previous studies have shown that during the spreading and approaching the host, zoospores can have complicated swimming patterns and behaviors as they experience multiple interactions with environmental signals, both physical, electrical and chemical, in soil and host-root surface[16]. For instance, potassium, which is uptaken by roots in the soil, reduces zoospore swimming speed, causes immediate directional changes and also results in perpetual circle trajectories [17, 18]. Bassani *et al.* provide transcriptomic studies showing that potassium induces zoospore aggregation, which facilitates the advantages for zoospores to attack the host-root [19].

* Current address: Université Paris-Saclay, CNRS, LPTMS, UMR8626, 91405 Orsay, France; duc-quang.tran@ijm.fr
† xavier.noblin@univ-cotedazur.fr

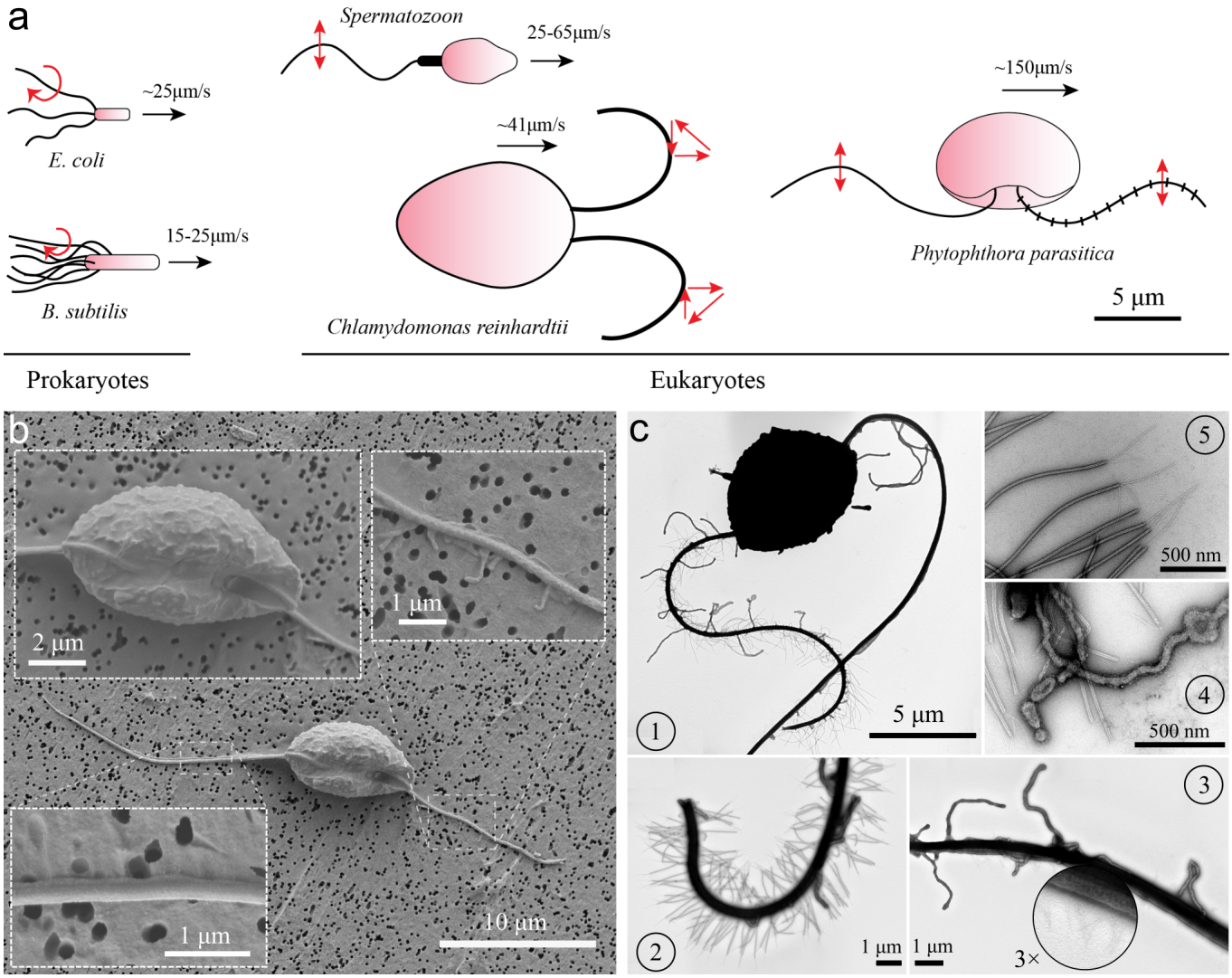

FIG. 1. Characteristics of *P. parasitica* zoospore. (a) Swimming of zoospores in comparison with different prokaryotic and eukaryotic microswimmers. Red arrows indicate the beating patterns of the flagella, black arrows indicate the swimming speed and direction of the swimmers. (b) SEM images of the zoospore. The insets show the enlarged images of the cell body and the two flagella. (c) TEM images with negative staining. (1) Image of the zoospore showing the different structures of the two flagella. The anterior has different mastigonemes in various sizes, while the posterior has a smooth straight structure. (2) Close zoom-in image of the anterior flagellum. It is noticed that there are two types of mastigonemes on this flagellum: one with straight tubular shape, the other with flimsy shape but longer and bigger in size. (3) Close zoom-in image of the posterior flagellum. There are plenty of thin and short hairs wrapping along the flagellum and several non-tubular mastigonemes appearing near the cell body. (4) The non-tubular mastigonemes. (5) The tubular mastigonemes with tiny hairs at the tip.

Experimental evidence has demonstrated that zoospore-zoospore interaction can lead to "pattern swimming", a microbial bioconvection happened without the appearance of chemical or electrical signals [20, 21]. These findings urge for a better understanding of the swimming physics of the individual zoospores and how the combination of their two heterogeneous flagella results in those complex swimming behaviors.

A zoospore is usually about $10\,\mu$m in size and has a kidney-like cell body [22, 23]. At least two unique traits distinguish zoospores from other prokaryotic and eukaryotic microswimmers currently studied using physical approaches: (i) The two flagella beat longitudinally along the anterior-posterior axis of the cell body and not laterally as in the case of the green algae *Chlamydomonas*; (ii) two flagella distinguished from each other as the anterior flagellum has a tinsel-like structure, while the posterior one has a smooth whiplash one, both beating periodically with wave propagation directions outwards the body. At first look, these two flagella seem to be competing each other due to the opposite wave propagation directions. In fact, they both generate thrust in the same direction and propel the cell body forwards thanks to the thrust reversal resulted from multiple mastigoneme structures on

the anterior flagellum [19, 24, 25]. In other microswimmers, their flagella are often synchronized to perform a cooperative swimming when they are a few microns away from each other [2, 26]. For examples, *C. reinhardtii* performs breaststroke swimming by two flagella drawing away and back to each other [4] or *E. coli*, *B. subtilis* bacteria's flagella form a bundle and rotate together like a corkscrew to propel the cell body [3]. The question that whether zoospores, as eukaryotic swimmers, possess the similar cooperative behaviors of their flagella is of good interest. It was previously claimed that zoospore flagella are independent on each other and able to perform different tasks. Carlile [27] describes that the anterior flagellum is responsible for pulling the zoospore through water whereas the posterior flagellum acts as a rudder for steering the cell. However, Morris *et al.* [28] observe *P. palmivora* zoospores stop momentarily and then self-orientate their bodies to a new direction relatively to the posterior flagellum. Nevertheless, the cooperative actions of the motor and rudder were not carefully observed nor investigated, which remains mysteries about how zoospores change direction and respond to chemical and physical environment. This underwhelming knowledge motivates us to unveil the physics behind individual swimming of zoospores.

In this article, we first investigate characteristics of zoospore trajectories at a global scale, then focus on the flagella scale's swimming mechanisms. We observe that zoospores can perform long and stable straight runs, discontinued by active turning events. We obtain statistics of the trajectories and develop a numerical model to study and extrapolate the zoospore spreading characteristics. Then, we detail an in-depth study on the hydrodynamics of *P. parasitica*'s flagella and acquire a mathematical model to correlate the functions of two flagella on the motion of straight runs. Moreover, we discover an unique active turning mechanism of the zoospores including a body rotation then steering to a new direction. Our study reveals the mechanism and characteristics of zoospore spreading, which provides better insights on understanding and control of *Phytophthora* diseases.

CHARACTERISTICS OF *P. PARASITICA'S* CELL BODY AND FLAGELLA

To understand the swimming, we first look at the cell body and flagellum structures of *P. parasitica*. By using Scanning Electron Microscopy (SEM), we are able to observe the shape of the cell body and the positions to where the flagella are attached (Figure 1(b)). The cell in general has an ellipsoidal shape with tapered heads and a groove along the body. The size of the body is measured to be $8.8\pm0.4\,\mu$m (SE) in length, and $4.7\pm0.1\,\mu$m (SE) in width. The anterior flagellum attaches to the cell body in a narrow hole at one side of the groove, possessing an average length of $15.5\pm0.1\,\mu$m (SE). The posterior flagellum has the same diameter as the anterior's ($0.3\,\mu$m) but it is longer ($20.3\pm0.76\,\mu$m (SE)), and attaches directly to the surface of the groove. The roots of two flagella are apart from each other with a distance of $2.9\pm0.1\,\mu$m (SE). Some mastigoneme structures were observed on the anterior flagellum, but could only be distinguished with difficulty by Scanning EM techniques.

Observing the zoospores with Transmission Electron Microscopy (TEM) after negative staining, we discover multiple mastigonemes on both flagella (Figure 1(c1-3)). There are 2 different types of mastigonemes on the anterior flagellum: (1) straight and tubular shape, high density (14-16 units per μm), $0.03\,\mu$m diameter, $1.5\,\mu$m long; (2) flimsy and non-tubular shape, longer and bigger in size ($0.1\,\mu$m diameter, $1.8\,\mu$m long), and randomly distributed (Figure 1(c2)). The posterior flagellum instead has a smooth whip shape with plenty of very fine hairs on the surface (Figure 1(c3)). These hairs wrap around the flagellum to increase the contact surface, thus increasing the propulsion efficiency [29]. We also see a few flimsy mastigonemes on the posterior flagellum but they only appear near the root. The function of type-2 mastigonemes (Figure 1(c4)) is unknown, but their flexibility and random arrangement suggest that they might not contribute to generate drag. In contrary, the type-1 mastigonemes (Figure 1(c5)) are tripartite hairs that occur in most of Stramenopiles kingdom. They are known to be able to generate increased drag and reverse thrust for the anterior flagellum [24, 30].

STATISTICS OF SWIMMING PATTERNS

We investigate the characteristics of zoospore swimming by analyzing their trajectories and behaviors in a duration of 60 s in water. To facilitate that, we perform microscopic assays where a low concentration of individual zoospores are released to an open thin film of water with thickness of $\sim$100 μm on a glass slide. The zoospore swimming is captured at 60 fps (interval time between two consecutive frames, $\Delta t \approx 0.0167\,$s). The images are processed by Fiji [31] using Trackmate plugin [32] to semi-automatically track the positions of zoospores during the experiment duration (the captured images are shown in Supp. Movie 1). **Figure 2**(a) illustrates the trajectories of zoospores captured from the microscopic assay. These trajectories indicate that zoospore can perform long and straight runs, some can even cross the whole observatory region. The straight runs are separated by multiple turning events when zoospores randomly change directions. With this swimming strategy, zoospores can be categorized as run-and-tumble active particles [33]. From the position data of each zoospore over time, we achieve its movement characteristics defined by two parameters: magnitude of speed U and moving directions θ (Figure 2(b) & (c)), after applying moving average method with step length $n = 12$ to improve the accuracy of moving direction and instantaneous speed of the zoospore. From U values, we can separate

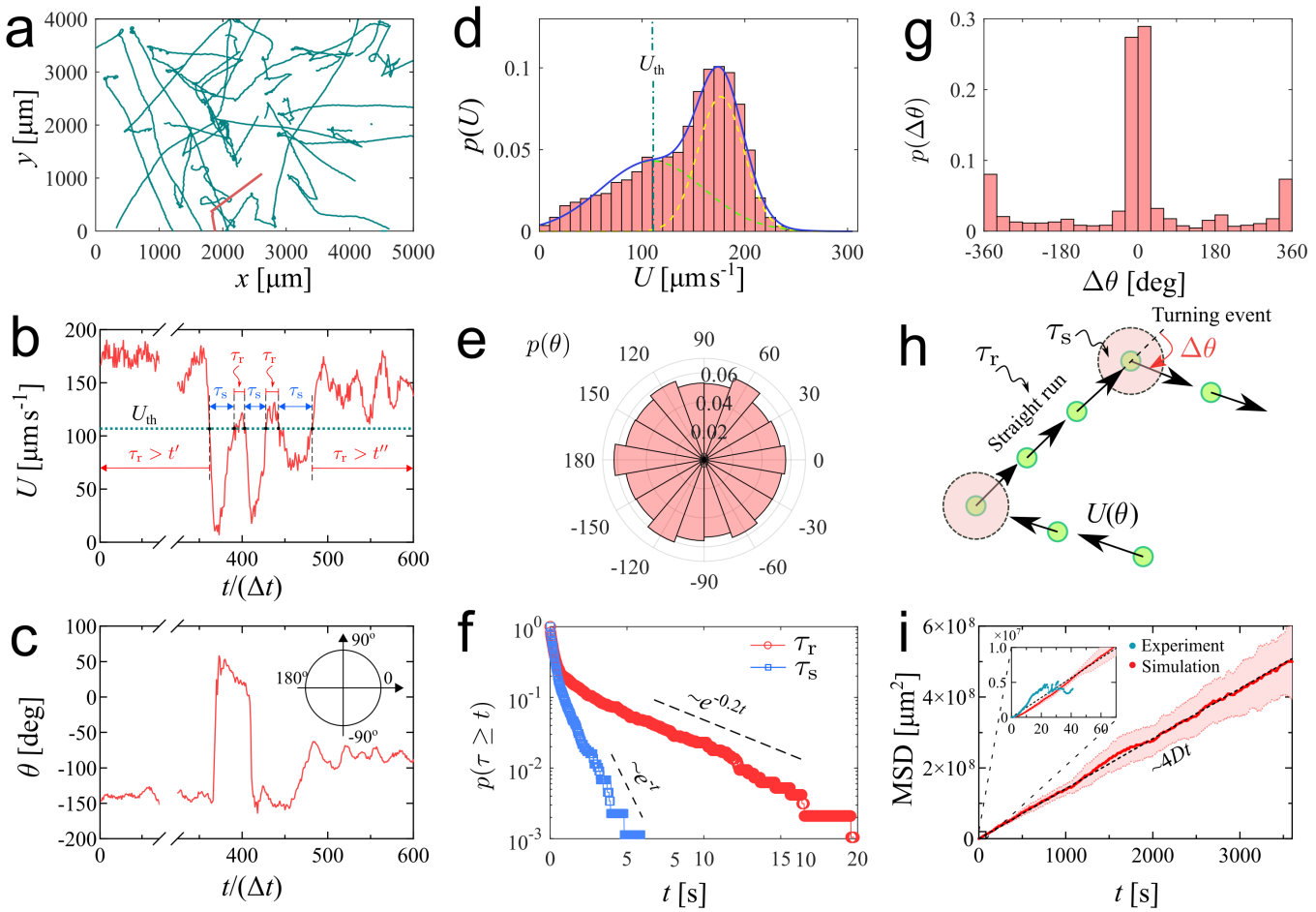

FIG. 2. Swimming trajectories of *P. parasitica* zoospores. (a) Trajectories of zoospores swimming in water captured from the microscopic assay for 60 s. Sample size $N = 58$. Note: not all trajectories are shown. Each position of the zoospores is captured every $\Delta t = 0.0167\,\mathrm{s}$. The trajectories are smoothed with moving average (step length $n = 12$). (b) The progression of speed U and (c) moving directions θ over time of a single zoospore extracted from the population in the assay. (d) Distribution of zoospore speed $p(U)$. (e) Polarity distribution of moving direction $p(\theta)$. (f) Survival curves $p(\tau \geq t)$ of the running time τ_r and stopping time τ_s. (g) Distribution of turning angle $p(\Delta\theta)$. (h) Schematics showing the strategy of the simulation model of zoospores swimming in water. (i) The estimated mean squared displacement (MSD) over time intervals t, constructed from the simulation data. The inset compares the experimental data and simulation of MSD at the experimental time-scale of 60s. By simulation, at long time scale of 1 hour, MSD of zoospores shows a diffusion of Brownian particles with the diffusion coefficient $D = 3.5 \times 10^{-4}\mathrm{cm}^2\,\mathrm{s}^{-1}$.

the movement of zoospores into 2 states: running state during straight runs and stopping state at turning events. While running, U and θ vary around a constant value. At turning events, U drops drastically, (occasionally close to 0) then quickly recover, θ also quickly changes to a new direction. U_th is defined as the threshold speed that separates the two states of running and turning. With U_th, we determine two important parameters of zoospore swimming: (1) running time τ_r as the duration when $U \geq U_\mathrm{th}$, deciding how long a zoospore is able to travel without turning; (2) stopping time τ_s as the duration when $U \leq U_\mathrm{th}$ for a zoospore to perform a turn.

We plot the distribution of U for all the trajectories of zoospores swimming in the observatory region for duration of 60 s (total number of zoospores $N = 60$) in Figure 2(d). The speed distribution $p(U)$ exhibits a combination of two different normal distributions: $f_1(U) = 0.082\,e^{-(U-\mu_1)^2/2\sigma_1^2}$ with $\mu_1 = 176.6$, $\sigma_1 = 22.3\,\mu\mathrm{m\,s}^{-1}$, and $f_2(U) = 0.043\,e^{-(U-\mu_2)^2/2\sigma_2^2}$ with $\mu_2 = 110$, $\sigma_2 = 53\,\mu\mathrm{m\,s}^{-1}$. This bimodal distribution of U indicates that zoospore speed fluctuates around two speed values $U = \mu_1$ and $U = \mu_2$, corresponding to two behavioral states of running and turning. The distribution f_1 is associated with the running state where zoospores experience stable moving speed, while f_2 represents the speed at turning events where zoospores reduce their speed from a stable running speed to 0 then quickly recover. We achieve the fitting curve for $p(U)$, resulted from the sum of two Gaussian fits $f_1 + f_2$, and choose the speed at inflection point of the fitting curve

where $\mu_s \leq U \leq \mu_r$ as the speed threshold to separate two behavioral states, $U_{th} = 111.5\,\mu m\,s^{-1}$. U_{th} at the inflection point determines a turning point for a significant change of the speed from running to turning state. We also plot the polarity distribution of zoospores in Figure 2(e) based on the moving direction θ and acquire an equally distributed in all directions. With the defined U_{th}, we calculate and plot the distributions of τ_r and τ_s in form of survival curves $p(\tau \geq t)$ in Figure 2(f). Both survival curves show complex behaviors of zoospores during running and turning. The statistics $p(\tau_s \geq t)$ can be considered as sum of two exponential decays with average stopping time $\bar{\tau}_s = 0.37\,s$. Also, $p(\tau_r \geq t)$ is in form of two exponential decays with average running time $\bar{\tau}_r = 1.0\,s$. We can estimate that zoospores stop and turn with the frequency $1/\bar{\tau}_r$ greater than $1\,Hz$ ($p(\tau_r < 1.0\,s) = 0.82$). Based on the moving direction over time, we calculate the average turning speed of zoospores at $\bar{\dot{\theta}} \approx 0.6\pi\,rad\,s^{-1}$. At each stopping time they perform a turning angle $\Delta\theta = \theta_i - \theta_e$, where θ_i and θ_e is the moving direction right before and after each turning event, respectively. The distribution of $\Delta\theta$ is shown in Figure 2(g), demonstrating the equal preference of turning directions (with positive angle values indicating counter-clockwise, and negative as clockwise direction). It is also shown that zoospores preferentially turn with the angle around 0°, which explains why they can have long and straight trajectories.

Since the motion of zoospore is characterized by the succession of of straight runs and turning events, as illustrated in Figure 2(h), in order to quantify their large-scale transport properties, we assemble all previous measurements in the following way. Each straight run is characterized by a speed $U_r > U_{th}$ and a duration τ_r drawn from the distributions in Figure 2(d) and Figure 2(f), respectively. After a run phase, an idle phase of duration τ_s, drawn from Figure 2(f) follows. The moving direction of the r-th run phase is given by $\cos(\theta_r)\hat{x} + \sin(\theta_r)\hat{y}$, i.e. it is parameterized by an angle θ_r. Note that moving direction of two consecutive r-th and $(r+1)$-th run phases are correlated. Moreover, $\theta_{r+1} = \theta_r + \Delta\theta$, where $\Delta\theta$ is a random angle drawn from the distribution in Figure 2(g). Mathematically, the position $\mathbf{x}_m$ of the zoospore after m run phases is given by $\mathbf{x}_m = \sum_{r=1}^{m} U_r\,\tau_r[\cos(\theta_r)\hat{x} + \sin(\theta_r)\hat{y}]$, and its mean-square displacement is $\mathrm{MSD}(m) = \langle(\mathbf{x}_m - \langle\mathbf{x}_m\rangle)^2\rangle$, where $\langle\cdots\rangle$ denotes average over realizations of the process. Our simulation results in a diffusive behavior of zoospores, with the MSD proportional to t. The diffusion coefficient is then obtained from $D = \lim_{m\to\infty} \frac{\mathrm{MSD}(m)}{4m(\langle\tau_r\rangle + \langle\tau_s\rangle)}$. In the computation of MSD and D, we assume that the only random variable exhibiting correlations is θ_r, while U_r, τ_r, and τ_s are uncorrelated. This procedure allows us to obtain a reliable estimate of D, with $D = 3.5 \times 10^{-4} cm^2\,s^{-1}$, which is in the same order of magnitude as the diffusion coefficient of *C. reinhardtii*'s [4]. We stress that direct measurements of D based on experimental MSD data are highly unreliable given the relatively small number of trajectories and their short duration, however, the data are enough to obtain reliable estimates on the distributions of $\Delta\theta$, U_r, τ_r, and τ_s from which, as explained above, D can be reliably estimated. Similar methods of using a theoretical random walk model to estimate the macroscopic parameters from the microscopic experiment have been previously developed for *C. reinhardtii* [34, 35].

ROLE OF TWO FLAGELLA COOPERATION IN SWIMMING MOTIONS OF ZOOSPORES

Our statistics study on swimming trajectories of zoospores has delivered characteristics of their movement at large scale, including the straight runs and turning events. These motions are controlled by two flagella oriented in opposite directions along the cell body's anterior-posterior axis. In this section, we look in-depth to how these two flagella cooperate to generate speed and perform turning for zoospores by conducting microscopy assays at small length scale of which the flagella are visible and in very short time scale.

Straight runs

We observe zoospores during their straight runs with visible flagella by conducting brightfield microscopy at $40\times$ objective with a high speed camera capturing at 4000 fps and exposure time at $200\,\mu s$. In Fig. 3(a), we show images of a *P. parasitica's* zoospore swimming by two flagella beating in sinusoidal shapes with the wave propagation in opposite directions. While translating, the cell body rotates around the moving direction simultaneously, which results in a helical swimming trajectory (see Supp. Movie 3 for a long run of a zoospore swimming in water). It has been shown that microswimmers with chiral shape of the body and asymmetric arrangement of their flagella are among the reasons causing this self rotational motion [26, 36, 37]. By quantifying the pitch of the helical trajectories, we achieve the rotational speed of the cell body approximately $3.5\pi\,rad\,s^{-1}$. This rotation also confirms that each flagellum of zoospores beat as a flexible oar in a 2D plane, because during the rotation, we observe at some points that the shapes of two flagella are flattened into two straight lines. Next, we retrieve the parameters of the beating flagella including beating frequencies f and wavelengths λ, by applying kymographs on the cross-sections within the two flagella and normal to the moving direction of the zoospore. We present more details of the parameter retrieval with kymographs in Supp. Materials. Our data show that when swimming in straight runs, the anterior flagellum of zoospores usually beats at $f_1 \approx 70\,Hz$ while the posterior flagellum beats faster with $f_1 \approx 120\,Hz$. We focus on a very short duration of less than $50\,ms$, which is equivalent to a translation of less than $10\,\mu m$. Compared with

the rotation motion at time-scale of 1 s, we can neglect the effect of the cell body's rotation during the straight runs.

We continue developing a mathematical model to study how the dynamics of beating flagella helps generating thrust for the cell to move forward. We assume that the rotation of the cell body does not affect the shapes and motions of the flagella as $U_{\mathrm{R}} << U_X$. Thus, the swimming zoospore can be considered as a 2D model (Fig. 3(b)) in which the cell body is an ellipse defined as $x^2/a^2 + y^2/b^2 = 1$ in its body-fixed frame (xOy), with the anterior and posterior flagellum having sine waveform shapes defined as

$$y(x,t) = A_k \sin\left(\omega_k t + (-1)^k \frac{2\pi\left[x + (-1)^k c\right]}{\lambda_k}\right) \quad (1)$$

as $(-1)^k x \leq -c$, where A_k is the amplitude, ω_k is the angular speed, λ_k is the wavelength of the anterior $(k = 1)$ and the posterior flagellum $(k = 2)$. The two flagella are attached to the cell body at two points both lying on x-axis and distanced to the origin O a gap of c, and beating with the wave propagation $\vec{v}_{\mathrm{w}}$ having directions against each other. The anterior has length L_1 and diameter d_1 while those of the posterior are L_2 and d_2. Additionally, there are multiple tubular mastigonmes with length h and diameter d_{m} attached to the surface of the anterior flagellum with density N_{m}. Note that, we ignore the effects of the flimsy mastigonemes in accumulating drag due to their non-tubular and random structures.

Zoospores swim in water with very low Reynolds number ($Re << 1$), resulting in negligible inertia, dominant viscous force and the kinetic reversibility [38, 39]. Microswimmers with flexible flagella generate thrust from drag force acted by fluid on the flagellum segments. In our model, we use Resistive Force Theory (RFT) to deal with the calculation of fluid's drag force on the two flagella of the zoospore. RFT has proven to be an effective and accurate method to predict the propulsive force and velocity of microswimmers regardless of the interactions of flagellum-flagellum or flagellum-body [40–43]. In case of zoospores where two flagella are in opposite directions, and the flagellum-body interaction is insignificant, RFT is a suitable solution to apply. Following this method, each flagellum is divided into infinite segments of length $\mathrm{d}s_k$, and each segment is located in the body-fixed frame (xOy) by a position vector $\vec{r}_k = x_k\vec{i} + y_k\vec{j}$, where $\vec{i}$, $\vec{j}$ are the unit vectors in x- and y-direction, respectively; x_k and y_k satisfy the shape equation (1) for the anterior $(k = 1)$ and the posterior $(k = 2)$.

RFT states that the drag force by fluid acting on an infinitesimal segment $\mathrm{d}s$ of the flagellum is proportional to the relative velocity of fluid to the flagellum segment,[40, 44, 45] as follows

$$\frac{\mathrm{d}\vec{F}}{\mathrm{d}s} = K_{\mathrm{N}} V_{\mathrm{N}} \vec{n} + K_{\mathrm{L}} V_{\mathrm{L}} \vec{l}, \quad (2)$$

where V_{N} and V_{L} are two components of relative velocity of fluid in normal and tangent direction to the flagellum segment, K_{N} and K_{L} are the drag coefficients of the flagellum in normal and tangent to the flagellum segment, $\vec{n}$ and $\vec{l}$ are the unit vectors normal and tangent to the flagellum segment, respectively. The drag coefficients K_N and K_L are estimated by Brennen and Winet [46], which depends on fluid viscosity, the wavelength and diameter of a flagellum.

We then apply RFT on each flagellum of the zoospore to calculate the total drag force accumulated. For the posterior flagellum, each segment $\mathrm{d}s_2$ is a simple smooth and slender filament (see inset $\mathrm{d}s_2$ in Fig. 3(b)), having drag coefficients K_{N2} and K_{L2}.

For the anterior flagellum, each segment $\mathrm{d}s_1$ contains additional $N\mathrm{d}s_1$ mastigonemes which are considered perpendicular to the segment itself (see inset $\mathrm{d}s_1$ of Fig. 3(b)). These mastigonemes also act as slender filaments accumulating drag from water. Interestingly, due to the direction arrangement, the relative velocity normal to the flagellum segment results in drag force in tangent direction to the mastigonemes, and subsequently, the relative velocity tangent to the flagellum segment results in drag force in normal direction to the mastigonemes. In another perspective, we can consider the anterior flagellum receives additional drag from the mastigonemes, which is presented by two increased drag coefficients in normal and tangent direction defined as

$$K_{\mathrm{N1}} = (K_{\mathrm{Nf1}} + N_{\mathrm{m}} h K_{\mathrm{Lm1}}) \quad (3)$$

and

$$K_{\mathrm{L1}} = (K_{\mathrm{Lf1}} + N_{\mathrm{m}} h K_{\mathrm{Nm1}}), \quad (4)$$

respectively. Here, N_{m} is the density of mastigonemes; h is the length of each mastigoneme; K_{Nf1} and K_{Lf1} are the drag coefficients in normal and tangent direction of the flagellum filament, respectively; K_{Nm1} and K_{Lm1} are the drag coefficients in normal and tangent direction of the mastigonemes, respectively.

In low Reynolds number condition, total forces equate to zero due to approximately zero inertia. Thus, we derive translational velocity U_X of the zoospore as shown in (5)

$$U_X = \frac{\frac{2\pi^2 K_{\mathrm{N1}} L_1 v_{\mathrm{w1}} (\gamma_1 - 1)\beta_1^2}{1+2\pi\beta_1^2} - \frac{2\pi^2 K_{\mathrm{N2}} L_2 v_{\mathrm{w2}} (\gamma_2 - 1)\beta_2^2}{1+2\pi\beta_2^2}}{K_{\mathrm{N1}} L_1 \left(\frac{\gamma_1 - 1}{1+2\pi\beta_1^2} + 1\right) + K_{\mathrm{N2}} L_2 \left(\frac{\gamma_2 - 1}{1+2\pi\beta_2^2} + 1\right) + 6\pi\mu b \xi_{\mathrm{e}}}, \quad (5)$$

where $v_{\mathrm{wk}} = \lambda_k f_k$ is the wave propagation velocity of the flagellum, $\gamma_k = K_{\mathrm{Lk}}/K_{\mathrm{Nk}}$ is the drag coefficient ratio, $\beta_k = A_k/\lambda_k$ is the flagellar shape coefficient, and ξ_{e} is the shape coefficient of the ellipse cell body. See Supp. Materials for the detail derivative.

We plot the value of U_X with different density of the mastigonemes, and varying the beating frequencies of the two flagella f_1 and f_2 in Fig. 3(c). The dimensions and physical parameters of the zoospore's cell body and two flagella are taken from Table S1. The plots show us that the appearance of mastigonemes results in a reversed thrust from the anterior flagellum. To illustrate

this, when $N_\mathrm{m} = 0$ (which means no mastigonemes) and $f_2 = 0$ (which means the posterior flagellum not beating), the anterior flagellum generates a thrust in negative X-direction giving a negative value of U_X. This agrees very well with the previous works stating a smooth reciprocal beating flagellum results in a propulsive velocity against direction of the wave propagation [40, 42, 44]. But since $N_\mathrm{m} > 2$, the velocity of the zoospore is reversed to positive X-direction due to the extra drag from the mastigonemes. This phenomenon was also described in hydrodynamics by Namdeo *et al.* [25], and observed in experiment of Cahill *et al.* [24]. However, it is also shown that the mastigoneme density should not be too high (more than 20 per 1 μm flagellum length) since they are not going to help increasing the speed any higher. We also notice that the mastigoneme density that we measure on zoospores by TEM is ranging from 14 to 18 per 1 μm flagellum length, which falls between the optimum range to generate the highest speed.

In Figure 3(d), we plot U_X with the variation of f_1 and f_2 while $N_\mathrm{m} = 15$, to show the influences of each flagellum on the zoospore speed. We find that given the same beating frequency, the anterior flagellum is able to generate higher propulsive thrust on the cell body than the posterior one. For instance, with the anterior flagellum beating at $f_1 = 100\,\mathrm{Hz}$ and the posterior flagellum being removed ($f_2 = 0$, $L_2 = 0$), the zoospore accumulates a speed of $\sim 270\,\mu\mathrm{m\,s^{-1}}$, while $f_2 = 100\,\mathrm{Hz}$ and $f_1 = 0$, $L_1 = 0$ result in a speed of $\sim 50\,\mu\mathrm{m\,s^{-1}}$. If the anterior flagellum increases f_1 to 120 Hz, it is able to singly induce a speed of $400\,\mu\mathrm{m\,s^{-1}}$. However, the posterior flagellum singly beating at $f_2 = 200\,\mathrm{Hz}$ only generates a speed of $90\,\mu\mathrm{m\,s^{-1}}$. Thus, we consider the anterior flagellum as the main motor of zoospores because it has the ability to significantly increase or decrease speed with a small adjustment of its beating frequency. In fact, we also observe zoospores swimming with the single beating anterior flagellum when they change directions (**Figure 4**(a)). Nevertheless, high-speed and additional drag from mastigonemes mean high power needed for the anterior flagellum to operate. We believe optimizing the energy consumption by reducing speed from the anterior flagellum and taking additional thrust from the posterior flagellum is important for zoospores to maintain their long-time exploration in nature. Moreover, as f_1 increases, the extra speed generated by the posterior flagellum decreases, which makes the propelling efficiency also decrease. Thus, zoospores should use both flagella with the anterior flagellum beating at lower frequency.

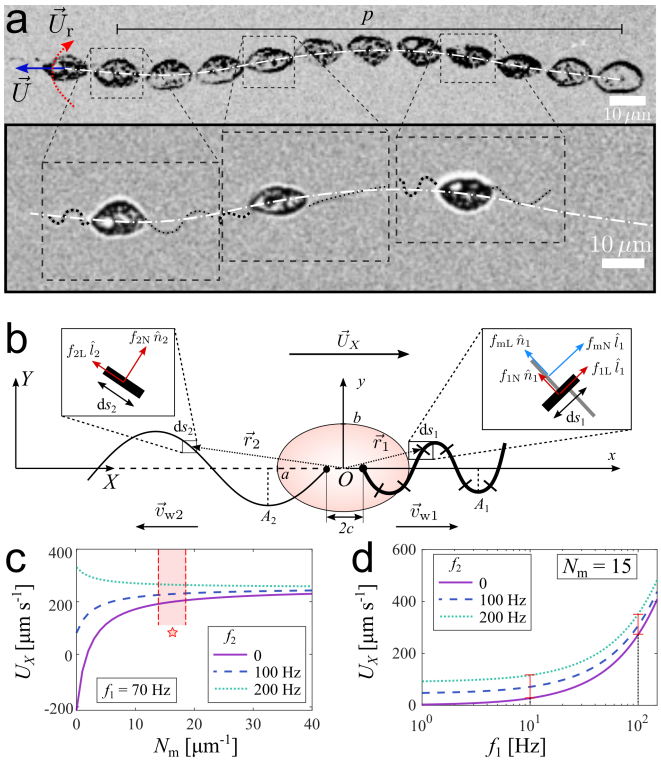

FIG. 3. Theoretical model of swimming individual *P. parasitica* zoospore. (a) Images of an individual zoospore swimming with two flagella beating in sine waveform shapes and its cell body rotating while moving forward. The combined motion results in a helical swimming trajectory. (b) Theoretical model of a zoospore translating in a 2D plane using Resistive Force Theory. (c) The dependence of translational velocity U_X on the tubular mastigoneme density (N_m), and (d) on the beating frequencies of two flagella (f_1 and f_2). The range of N_m with symbol ($\star$) indicates the values measured by TEM.

Turning events

We capture zoospores changing their directions by a unique active turning mechanism and an interesting cooperation between two flagella (Figure 4(a)). At first, to prepare for the turn, zoospores are observed to reduce their speed, then perform a quick body rotation while the posterior flagellum stops beating (Figure 4(a1-3)). Interestingly, right after the rotation, the anterior flagellum switches to beating singly to drag the body to a new direction while the posterior flagellum is still immobile (Figure 4(a4-5)). Finally, the posterior flagellum resumes its beating for the zoospore to achieve a stable direction (Figure 4(a6)). The movies of zoospore turning are captured at 2000 fps with the same setup as the microscopic assay (see Supp. Movie 4). Using Fiji and Trackmate, we track the positions of the zoospore and plot the trajectory, smoothed by moving average with $n = 40$, during its turning event. Figure 4(b) presents trajectory of the zoospore in Figure 4(a), showing multiple circular motions during turning before the zoospore changes to a new direction. We then compute the zoospore speed U (Figure 4(c)), and the moving directions θ from the trajectory while manually measure body orientation ψ over time (Figure 4(d)). The data of U shows that zoospores slowly reduce speed, then quickly perform a turn. Looking at the turning duration τ_s, it is shown that the zoospore

speed U consists of two patterns: (i) fluctuation at high magnitudes and low frequencies indicating the body rotation, then switch to (ii) steering with fluctuation at low magnitudes and high frequencies. These two patterns can also be distinguished by the difference between the moving direction θ and the body orientation ψ. The anterior flagellum plays an important role in turning events in addition to straight runs. As the posterior flagellum stays immobile, all the movement of zoospores during turning, including the body rotation and the steering, is produced by the anterior flagellum. Due to the limitation in 2D observation, we are not able to observe the 3D shape of the anterior flagellum during the body rotation. We hypothesize that the anterior flagellum may switch its swimming pattern in order to achieve a new moving direction at a short time-scale of milliseconds. The turning ends when the zoospore recovers its speed and both its moving direction and body orientation emerge at the same value. Interestingly, after the turning ends, the anterior flagellum solely beats at a higher frequency and accumulates a high-speed of $\sim 250\,\mu\mathrm{m\,s}^{-1}$. The posterior resumes its beating, which is marked by the decrease of speed and the swimming is back to normal. We confirm that the posterior flagellum of zoospores does not act as a rudder to steer the direction. Instead, it is fully stretched during turning events and contributes to increase drag at one end of the cell body, which can create a fixed point, like an anchor for the body rotation and result in a sharp turning angle. The advantage of this turning mechanism is that it allows the zoospores to actively and quickly achieve a new direction, which is not the case of other microswimmers such as the tumbling of *E. coli*'s [47, 48] or *Chlamydomonas*'s [4, 49].

This visualization confirms the statement from Morris et al. [28] that the posterior flagellum of zoospores does not act as a rudder to steer the direction. The body itself actively changes to a new direction and the anterior flagellum steers the body to a new direction. We observe that the anterior flagellum also plays an important role in turning events in addition to the straight runs. As the posterior flagellum stays immobile, all the movement of zoospores during turning, including the body rotation and the steering, is produced by the anterior flagellum. Looking at the turning duration τ_s in Fig. 4(c), it is shown that the zoospore speed U consists of two patterns: (1) fluctuation at high magnitudes and low frequencies indicating the body rotation, then switch to (2) steering with fluctuation at low magnitudes and high frequencies. Due to the limitation in 2D observation, we are not able to observe the 3D shape of the anterior flagellum during the body rotation. The posterior flagellum acts like an anchor during this turning event to create a fixed point for the turning. The advantage of this turning mechanism is that it allows the zoospores to actively and quickly achieve a sharp turning angle, which is not the case of other microswimmers such as the tumbling of *E. coli*'s [47, 48] or *Chlamydomonas*'s [4, 49].

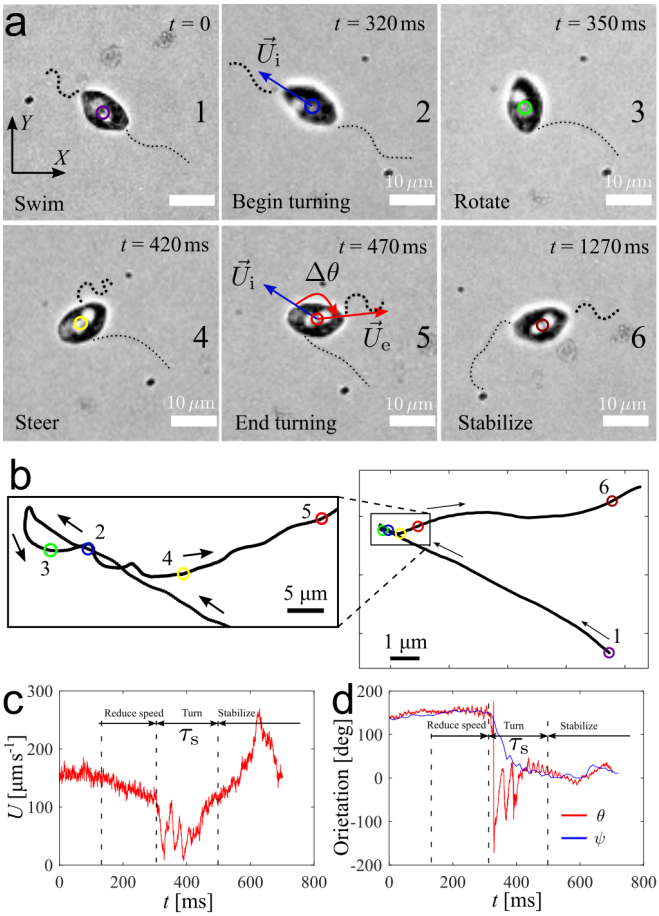

FIG. 4. Active turning of individual *P. parasitica* in water. (a) Images of a zoospore changing direction. The two flagella cooperate to help the cell body rotate and steer to a new direction achieving a turning angle $\Delta\theta$. (b) Trajectory of the zoospore during the turning event. (c) The speed U of the zoospore during the turning event. The turning starts when the speed begins to fluctuate with large magnitude and lower frequency, and lasts for a duration of τ_s with a rotation of the cell body followed by steering to the new direction. (d) The moving directions θ and the body orientation ψ of the zoospore during the turning event.

CONCLUSION

We have performed the fist systematic study of the swimming pattern and spreading features of *P. parasitica* zoospores, a plant pathogen, which is considered a major agricultural threat. Combining high-speed imaging and Resistive Force Theory, we showed how the two opposite flagella cooperate in producing thrust by beating together, allowing the microorganism to achieve high-speed swimming during straight runs. Furthermore, we found that steering is an coordinated process, in which the the posterior flagellum stops beating, while the anterior flagellum actively moves causing the cell body to rotate. Finally, we explain how fast-swimming periods and active turning events combine to produce a diffusion

coefficient of $D = 3.5 \times 10^{-4}\,\mathrm{cm}^2\,\mathrm{s}^{-1}$, a quantity that characterizes spatio-temporal spreading of this pathogen during plant epidemics.

It is worth stressing the motility pattern exhibited by the zoospores represents an Eukaryotic version of the "run-and-tumble" motility class exhibited by bacteria peritrichous bacteria. Several eukaryotic swimmers, e.g. spermatozoa, do not exhibit such kind of motility pattern, but *Chlamydomonas reinhardtii* have been reported to also fall into this category [4]. There are, however, important differences. *Chlamydomonas* possess two identical flagella located at one tip of the cell. Reorientation events occur during asynchronous beating periods of the two identical flagella, while straight runs require synchronous beating. In sharp contrast to this picture, we show that in zoospores while straight runs also involve a coordinated beating of the opposite and different flagella, turning requires the posterior flagellum to halt, while the anterior one continue beating. This strongly suggests that *P. parasitica* navigates using a fundamentally different internal regulation mechanism to control swimming, than *C. reinhardtii*, a mechanism that is likely to be present in other Eukaryotic swimmers with two opposite and different flagella.

MATERIALS AND METHODS

P. parasitica mycelium culture and zoospore release

We culture mycelium of *Phytophthora parasitica* (isolate 310, *Phytophthora* INRA collection, Sophia-Antipolis, France) [18, 19] routinely on malt agar at 24°C in the dark. To produce zoospores, we prepare the mycelium which is grown for one week in V8 liquid medium at 24°C under continuous light. The material was then drained, macerated and incubated for a further four days on water agar (2%) to induce sporangiogenesis. Zoospores are released from sporangia by a heat shock procedure. We place a petri-dish of mycelium inside a refrigerator at 4 °C for 30 minutes, then pour 10 ml of 37 °C distilled water on top of the mycelium and continue to incubate it at room temperature (25 °C) for another 30 minutes. Zoospores escape from sporangia and swim up to the water. The zoospore suspension is then collected for further experiments.

Scanning Electron Microscopy and Transmission Electron Microscopy with negative staining

For scanning electron microscopy (SEM) and transmission electron microscopy (TEM), cell pellets are fixed with in a 2.5 % glutaraldehyde solution in 0.1 M sodium cacodylate buffer (pH 7.4) at room temperature ($\sim$ 25 °C) for 1 hour and then stored at 4 °C. For SEM observations, after three rinsing in distilled water, protists are filtered on a 0.2 μm isopore filter. Samples on filters are subsequently dehydrated in a series of ethanol baths (70 %, 96 %, 100 % three times, 15 minutes each). After a final bath in hexamethyldisilazane (HMDS, 5 minutes), samples are left to dried overnight. Samples on filters are mounted on SEM stubs with silver paint and coated with platinum (3 nm) prior to observing. SEM observations are performed with a Jeol JSM-6700F SEM at an accelerating voltage of 3 kV.

For TEM observations, samples are prepared using the negative staining method. After three rinsing in distilled water, a drop of cells suspension ($\sim$10 μl) is left for 5 minutes on a TEM copper grid (400 mesh) with a carbon support film. The excess liquid is removed with a filter paper. Subsequently, staining is done by adding a drop of 0.5 % (w/v) aqueous solution of uranyl acetate on the grid for 1.5 minute, followed by removal of excess solution. The TEM observations are carried out with a JEOL JEM-1400 transmission electron microscope equipped with a Morada camera at 100 kV.

Microscopic assays of zoospores

We pipette a droplet of 10 μl water containing zoospores onto a microscopic glass slide and spread the droplet to thoroughly cover the marked area of 1×1 cm and become a thin film of approximately 100 μm thickness. We do not cover the droplet to prevent the unwanted interactions between the zoospores and rigid surface of coverslips. We observe the swimming of individual zoospores inside the flattened droplet under a bright field transmission microscope (Nikon Eclipse T*i*2, Minato, Tokyo, Japan) at 40× objective with the high speed camera Phantom v711 (Vision Research, NJ, USA). For the experiment to observe the swimming trajectories of the zoospores, we use 4× objective to capture a large swimming region of $5000 \times 4000\,\mu$m. The captured images are processed by Fiji with the Trackmate plugin.

Estimation of trajectory parameters

An individual zoospore positions are captured at each time frame Δt. At each $t_j = j\Delta t$ ($j = 1, 2, 3, ...$), the zoospore has a position $z_j = (x(t_j), y(t_j))$. First, we smooth the trajectory by moving average with step n. The smoothed positions $Z_{j,n}$ are calculated as

$$Z_{j,n} = \frac{1}{n} \sum_{j}^{n+j-1} z_j.$$

Each new position $Z_{j,n}$ possesses a velocity vector with speed

$$U_{j,n} = \frac{1}{\Delta t} \parallel z_{j+n} - z_j \parallel,$$

and moving direction (angle between velocity vector and x-axis)

$$\theta_j = atan\left(\frac{y_{j+n} - y_j}{x_{j+n} - x_j}\right).$$

ACKNOWLEDGMENTS

This work has been supported by the French government through the UCA^{JEDI} Investments in the Future project managed by the National Research Agency with the reference number ANR-15-IDEX-01. CCMA electron microscopy equipments have been funded by the Région Sud - Provence-Alpes-Côte d'Azur, the Conseil Général des Alpes Maritimes, and the GIS-IBiSA. We thank Marcos and David Gonzalez-Rodriguez for reading the manuscript and giving valuable feedback.

1. A. Ghanbari, *J Micro-Bio Robot*, 2020.
2. E. Lauga and R. E. Goldstein, *Phys. Today*, 2012, **65**, 30.
3. L. Turner, W. S. Ryu and H. C. Berg, *J. Bacteriol.*, 2000, **182**, 2793–2801.
4. M. Polin, I. Tuval, K. Drescher, J. P. Gollub and R. E. Goldstein, *Science*, 2009, **325**, 487–490.
5. D. R. Mitchell, *J Phycol*, 2000, **36**, 261–273.
6. S. Ishijima, S. Oshio and H. Mohri, *Gamete Res.*, 1986, **13**, 185–197.
7. S. T. Mortimer, D. Schevaert, M. A. Swan and D. Mortimer, *Hum. Reprod.*, 1997, **12**, 1006–1012.
8. F. Burki, *Cold Spring Harb. Perspect. Biol.*, 2014, **6**, a016147.
9. R. Derelle, P. López-García, H. Timpano and D. Moreira, *Mol. Biol. Evol.*, 2016, **33**, 2890–2898.
10. S. Kamoun, O. Furzer, J. D. Jones, H. S. Judelson, G. S. Ali, R. J. Dalio, S. G. Roy, L. Schena, A. Zambounis, F. Panabières *et al.*, *Mol. Plant Pathol.*, 2015, **16**, 413–434.
11. L. Derevnina, B. Petre, R. Kellner, Y. F. Dagdas, M. N. Sarowar, A. Giannakopoulou, J. C. De la Concepcion, A. Chaparro-Garcia, H. G. Pennington, P. Van West *et al.*, *Philos. Trans. Royal Soc. B*, 2016, **371**, 20150459.
12. A. Drenth and B. Sendall, *Diversity and management of Phytophthora in Southeast Asia. ACIAR Monograph*, 2004, 10–28.
13. R. N. Strange and P. R. Scott, *Annu. Rev. Phytopathol.*, 2005, **43**, year.
14. H. S. Judelson and F. A. Blanco, *Nat. Rev. Microbiol.*, 2005, **3**, 47.
15. F. Panabieres, G. S. Ali, M. B. Allagui, R. J. Dalio, N. C. Gudmestad, K. Marie-Line, G. Sanjoy, L. Schena and A. Zampounis, *Phytopathol. Mediterr.*, 2016, **55**, 20–40.
16. I. Bassani, M. Larousse, Q. D. Tran, A. Attard and E. Galiana, *Comput. Struct. Biotechnol. J.*, 2020, **18**, 3766–3773.
17. A. A. Appiah, P. Van West, M. C. Osborne and N. A. Gow, *Fungal Genet. Biol.*, 2005, **42**, 213–223.
18. E. Galiana, C. Cohen, P. Thomen, C. Etienne and X. Noblin, *J. R. Soc. Interface*, 2019, **16**, 20190367.
19. I. Bassani, C. Rancurel, S. Pagnotta, F. Orange, N. Pons, K. Lebrigand, F. Panabières, L. Counillon, X. Noblin and E. Galiana, *Microorganisms*, 2020, **8**, 1012.
20. N. Ochiai, M. I. DragIila and J. L. Parke, *Fungal biology*, 2011, **115**, 228–235.
21. A. I. M. Savory, L. J. Grenville-Briggs, S. Wawra, P. van West and F. A. Davidson, *J. R. Soc. Interface*, 2014, **11**, 20140017.
22. H. J. Mitchell, K. A. Kovac and A. R. Hardham, *Mycol. Res.*, 2002, **106**, 1211–1223.
23. C. A. Walker and P. van West, *Fungal Biol. Rev.*, 2007, **21**, 10–18.
24. D. M. Cahill, M. Cope and A. R. Hardham, *Protoplasma*, 1996, **194**, 18–28.
25. S. Namdeo, S. Khaderi, J. den Toonder and P. Onck, *Biomicrofluidics*, 2011, **5**, 034108.
26. B. M. Friedrich and F. Jülicher, *Phys. Rev. Lett.*, 2012, **109**, 138102.
27. M. Carlile, *Phytophthora: Its Biology, Taxonomy, Ecology and Pathology*, 1983, 95–107.
28. B. Morris, B. Reid and N. Gow, *Microbiology*, 1995, **141**, 1231–1237.
29. R. E. Lee, *Phycology*, Cambridge university press, 4th edn., 2018.
30. J. D. Dodge, *The fine structure of algal cells*, Elsevier, 2012.
31. J. Schindelin, I. Arganda-Carreras, E. Frise, V. Kaynig, M. Longair, T. Pietzsch, S. Preibisch, C. Rueden, S. Saalfeld, B. Schmid *et al.*, *Nat. Methods*, 2012, **9**, 676.
32. J.-Y. Tinevez, N. Perry, J. Schindelin, G. M. Hoopes, G. D. Reynolds, E. Laplantine, S. Y. Bednarek, S. L. Shorte and K. W. Eliceiri, *Methods*, 2017, **115**, 80–90.
33. M. Khatami, K. Wolff, O. Pohl, M. R. Ejtehadi and H. Stark, *Sci. Rep.*, 2016, **6**, 1–10.
34. N. Hill and D.-P. Häder, *J. Theor. Biol.*, 1997, **186**, 503–526.
35. V. Vladimirov, T. Pedley, P. Denissenko, S. Zakhidova *et al.*, *J. Exp. Biol.*, 2004, **207**, 1203–1216.
36. E. E. Keaveny and M. J. Shelley, *Phys. Rev. E*, 2009, **79**, 051405.
37. S. Namdeo, S. Khaderi and P. Onck, *Proc. Royal Soc. A*, 2014, **470**, 20130547.
38. E. M. Purcell, *Am. J. Phys*, 1977, **45**, 3–11.
39. T. Qiu, T.-C. Lee, A. G. Mark, K. I. Morozov, R. Münster, O. Mierka, S. Turek, A. M. Leshansky and P. Fischer, *Nat. Commun.*, 2014, **5**, 5119.
40. J. Gray and G. Hancock, *J. Exp. Biol.*, 1955, **32**, 802–814.
41. J. B. Y. Koh and Marcos, *Microfluid. Nanofluid.*, 2014, **17**, 613–622.
42. E. Lauga and T. R. Powers, *Rep. Prog. Phys.*, 2009, **72**, 096601.
43. Marcos, N. P. Tran, A. R. Saini, K. C. H. Ong and W. J. Chia, *Microfluid. Nanofluid.*, 2014, **17**, 809–819.
44. G. Hancock, *Proc. Royal Soc. A*, 1953, **217**, 96–121.

45. J. B. Koh, X. Shen and Marcos, *Microfluid. Nanofluid.*, 2016, **20**, 98.
46. C. Brennen and H. Winet, *Annu. Rev. Fluid Mech.*, 1977, **9**, 339–398.
47. N. C. Darnton, L. Turner, S. Rojevsky and H. C. Berg, *Journal of bacteriology*, 2007, **189**, 1756–1764.
48. E. P. Ipiña, S. Otte, R. Pontier-Bres, D. Czerucka and F. Peruani, *Nat. Phys.*, 2019, **15**, 610–615.
49. R. R. Bennett and R. Golestanian, *J. R. Soc. Interface*, 2015, **12**, 20141164.